Journal of Magnetism and Magnetic Materials 340 (2013) 38–45

Contents lists available at SciVerse ScienceDirect

Journal of Magnetism and Magnetic Materials

journal homepage: www.elsevier.com/locate/jmmm

Effect of Mg substitution on electromagnetic properties of NiCuZn ferrite

Ch. Sujatha [a,*], K. Venugopal Reddy [a], K. Sowri Babu [a], A. RamaChandra Reddy [a], M. Buchi Suresh [b], K.H. Rao [c]

[a] Department of Physics, National Institute of Technology, Warangal 506004, Andhra Pradesh, India
[b] Center for Ceramic Processing, ARC-International Balarpur, Hyderabad 500005, Andhra Pradesh, India
[c] Department of Physics, RGU-IIIT Nuzvid, Nuzvid 521201, Andhra Pradesh, India

ARTICLE INFO

Article history:
Received 1 August 2012
Received in revised form
17 March 2013
Available online 28 March 2013

Keywords:
Sol–gel method
Permeability
Dielectric property
Ferrite
Spinel

ABSTRACT

Mg substituted NiCuZn ferrites were prepared through sol–gel method using polyvinyl alcohol (PVA) as a chelating agent. The samples after annealing at 500 °C to remove PVA were sintered at 950 °C for 1 h. The structural and electromagnetic properties of the samples were investigated. All the samples showed single phase spinel structure with increased lattice constant as a function of Mg concentration. The morphology reveals polyhedral shaped grains with increased grain size as a function of Mg composition. Dielectric parameters showed low values at higher frequencies. The initial permeability increased with Mg substitution in place of Ni in accordance with the microstructure. The samples sintered at low temperature having low dielectric losses and improved permeability along with the high frequency stability of permeability find applications in multilayer chip inductors.

1. Introduction

Polycrystalline spinel ferrites are widely used in many electronic devices because of their high electrical resistivity, chemical stability, mechanical hardness and also they are available at low cost [1]. It is a well known fact that the properties of ferrites are sensitive to method of preparation, substitution of cations, microstructure, sintering time, temperature and mostly on distribution of cations on the tetrahedral (A) and octahedral sites (B) in the spinel lattice with the general formula AB_2O_4 [2]. Recently, surface mounting devices (SMD) have been rapidly developed for electronic applications, such as multilayer chip inductors (MLCIs) [3]. These are produced by coating ferrite and silver (Ag) electrode layers alternately and then co-firing them. The main requirements of MLCIs are good quality factor, high electrical resistivity, and high magnetic permeability in order to reduce the number of layers. Reduced number of layers in MLCIs was advantageous in minimising the capacity between the layers and realizing the miniaturisation of the electronic components [4,5]. Besides that low sintering temperature is necessary for avoiding diffusion of Ag (<961 °C—melting point of Ag) into the ferrites which adversely affects the electrical resistivity [6]. NiCuZn ferrite system is one of the soft magnetic material best suitable for MLCIs because of its low sintering temperature for densification and high permeability as well as high electrical resistivity in radio frequency (RF) range [7]. Numerous studies have been devoted on NiCuZn ferrites in enhancing the material properties suitable for MLCI applications [1,3,6–8]. Even though NiCuZn ferrite is the best suitable material for MLCIs, there are other magnetic properties (like magnetostriction constant) that disfavour use of these materials for MLCIs. NiCuZn ferrite system having high magnetostriction constant is sensitive to stress thereby affecting the magnetic properties [8]. In addition to that, Ni and its oxides produce carcinogenic effects on the environment and the precursors for Ni are expensive [9]. Nowadays attention is paid towards MgCuZn ferrites for MLCIs applications since these materials also exhibit good electromagnetic properties such as high resistivity, permittivity, permeability, high Curie temperature same as that of NiCuZn ferrites and are insensitive to stress due to their low magnetostriction constant [8,10].

John Berchmans et al. [11] and Naeem et al. [12] discussed the structural and electrical properties of Mg substituted $NiFe_2O_4$ system processed through wet chemical route methods. The cation distribution of NiMg ferrite system was examined through XPS and Mossbauer spectral analysis and they found that the percentage of Mg at tetrahedral site was maximum when the Ni content in the spinel was maximum [13]. Singh et al. [14] reported that substitution of Mg in place of Ni in NiZn ferrite has propitious results of improvement in both the electrical and magnetic properties. Rezlescu et al. [15] investigated MgCuZn ferrite with excess MgO in the composition to avoid divalent iron ions as well as discontinuous grain growth.

Varalaxmi et al. [16] observed improved initial permeability and reduced Curie temperature with the substitution of Mg in NiCuZn ferrite. Roy and Bera [17] investigated the effect of Mg on electromagnetic properties of NiCuZn ferrites for MLCIs applications and they found that up to a certain concentration of

* Corresponding author. Tel.: +91 870 2462560, mobile: +91 9502899683; fax: +91 870 2459547.
E-mail addresses: sujatha.phys09@gmail.com, chsuji2@gmail.com (Ch. Sujatha).

0304-8853/$ - see front matter © 2013 Elsevier B.V. All rights reserved.
http://dx.doi.org/10.1016/j.jmmm.2013.03.027

Mg ($x=0.18$) both the electrical resistivity and initial permeability increased. Su et al. [18] studied electromagnetic properties of NiMgCuZn ferrite prepared through conventional ceramic technique and the results demonstrated high frequency permeability suitable for MLCIs applications. Gabal [19] succeeded in preparing $Ni_{0.5-x}Cu_{0.2}Zn_{0.3}Mg_xFe_2O_4$ ferrite using egg white as a precursor and showed improved magnetisation with Mg substitution. Recently Abdullah Dara et al. [20] re-examined the above mentioned composition but prepared through sol–gel method and the results showed increased electrical resistivity and reduced dielectric losses with Mg substitution. In the present paper, detailed analysis of structure and morphology as well as dielectric and magnetic properties, especially frequency dispersion of permeability up to 50 MHz for $Ni_{0.5-x}Mg_xCu_{0.05}Zn_{0.45}Fe_2O_4$ composition processed through sol–gel method, is discussed.

2. Experimental procedure

$Ni_{0.5-x}Mg_xCu_{0.05}Zn_{0.45}Fe_2O_4$ nanoparticles were processed through sol–gel method. Analytical grade nickel, magnesium, zinc, copper and ferric nitrates were weighed in stoichiometric proportions and were dissolved separately in deionised water. Thus obtained cationic solutions were mixed one into another and stirred continuously for 1 h to improve homogeneity and the cationic solution is taken to be the precursor. The ratio of metal nitrates to polyvinyl alcohol (PVA) was maintained at 1:3. The required quantity of PVA was dissolved in deionised water slowly to get transparent clear solution. The precursor is mixed with PVA solution under constant stirring and heating. The gelation continued step by step till a red gel type product was formed with the release of reddish brown gases at about 100 °C, leaving the fluffy mass in the reaction vessel. The as dried powder was annealed at a temperature of 500 °C for 3 h. The annealed samples were then compacted in the form of pellets and toroids using polyvinyl alcohol as a binder and sintered at 950 °C for 1 h with a heating rate of 2 °C/min in a programmable muffle furnace.

2.1. Characterisation

The formation of spinel structure of the $Ni_{0.5-x}Mg_xCu_{0.05}Zn_{0.45}Fe_2O_4$ ferrite samples was investigated using an X-ray diffractometer with Co-Kα radiation (1.78897 A°) as a source. Crystallite size and lattice constant were determined by considering peak width and peak position of the reflections collected from an INEL XRG 3000 powder diffractometer in the 2θ range from 20° to 120°. Vibrational frequencies of tetrahedral and octahedral metal oxygen bonds were noted from Fourier Transform Infrared spectra (BRUKER OPTICS TENSOR 27) recorded in the wave number range 4000–400 cm^{-1} by preparing the sample in the form of thin transparent pellet by mixing with KBr. The microstructure and grain size distribution of nanoparticles having gold with palladium coated surfaces were investigated by a field emission scanning electron microscope (FESEM) Carl Zeiss Ultra 55 operating at an accelerating high tension voltage EHT of 17 kV. Room temperature static magnetisation measurements were carried out using vibrating sample magnetometer (EV-7VSM) with a maximum applied field of 15 kOe. The frequency dispersion of permeability for the sintered samples was measured using a high frequency LCR metre (WAYNKERR 6500P) in the frequency range of 20 Hz–50 MHz. Room temperature dielectric measurements on the disc shaped samples were carried out in the frequency range from 100 Hz to 5 MHz using an impedance analyzer (Solartron SI1260, Ametek, Inc., Hampshire, UK).

3. Results and discussion

3.1. X-ray diffraction (XRD)

Fig. 1 shows XRD patterns for the sintered $Ni_{0.5-x}Mg_xCu_{0.05}Zn_{0.45}Fe_2O_4$ ($x=0.1$, 0.2, 0.3 and 0.4) ferrite samples. The highest intensity peak around the diffraction angle (2θ) equal to 41° corresponding to (311) plane confirms the formation of cubic spinel ferrite. The observed XRD reflections in a pattern match well with the standard JCPDS File no. 08-0234 ($NiZnFe_2O_4$). There are no additional peaks related to secondary phase found in the XRD patterns, ensuring phase purity. The observed reflections in the XRD patterns are strong and sharp, indicating high crystallinity of the samples. All the structural parameters obtained from the XRD pattern are discussed in the next paragraph.

Accurate estimation of lattice constant has been done using the Nelson–Riley (NR) extrapolation method by minimising both systematic and random errors. The values of the lattice parameter obtained from each reflected plane were plotted against the NR function $F(\theta)$ [21]:

$$F(\theta)=\frac{1}{2}\left[\frac{\cos^2\theta}{\sin\theta}+\frac{\cos^2\theta}{\theta}\right]$$

A straight line graph was obtained. Extrapolation of the straight line to $F(\theta)=0$ or $\theta=90°$ gives an accurate lattice constant. With Mg substitution the lattice constant increases slightly, indicating that magnesium enters into the spinel lattice. This is due to the ionic radii differences of Mg^{2+} (0.72 Å) and Ni^{2+} (0.69 Å).

The theoretical X-ray density for the samples having spinel structure with 8 molecules per unit cell was calculated using the relation

$$d_{theoretical}=\frac{8M}{N_a a^3}$$

where M is the molecular weight, N_a is the Avogadro's number and a is the lattice constant.

The bulk density calculated by considering mass and dimensions of the disc shaped pellets is

$$d_{Bulk}=\frac{\text{mass}}{\pi r^2 t}$$

The compositional variation of both theoretical X-ray density and bulk density is shown in Fig. 2. The X-ray density was observed to be greater than the bulk density, but both are showing

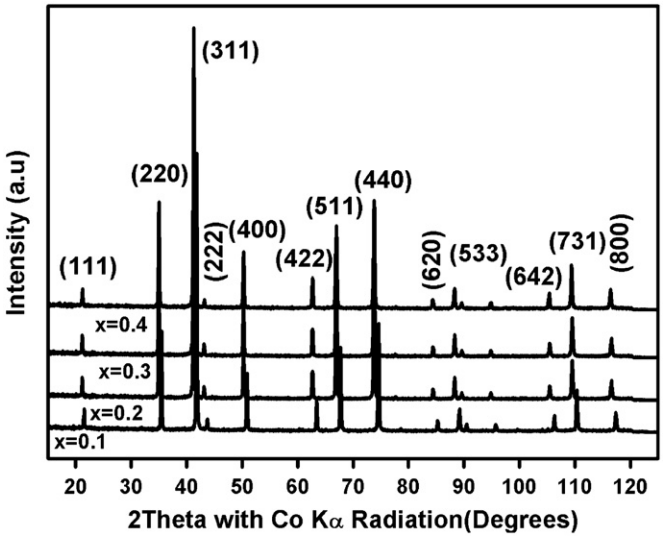

Fig. 1. X-Ray diffraction patterns for the $Ni_{0.5-x}Mg_xCu_{0.05}Zn_{0.45}Fe_2O_4$ ($x=0.1$, 0.2, 0.3, and 0.4) ferrite samples sintered at 950 °C.

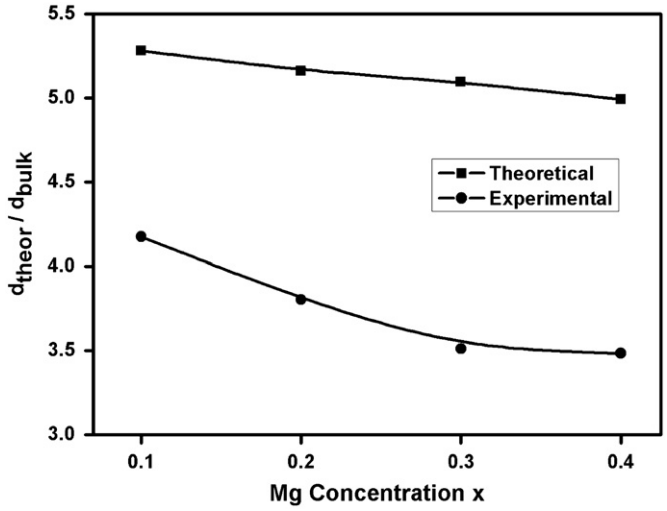

Fig. 2. Variation in X-ray density and bulk density of $Ni_{0.5-x}Mg_xCu_{0.05}Zn_{0.45}Fe_2O_4$ ferrite with Mg composition.

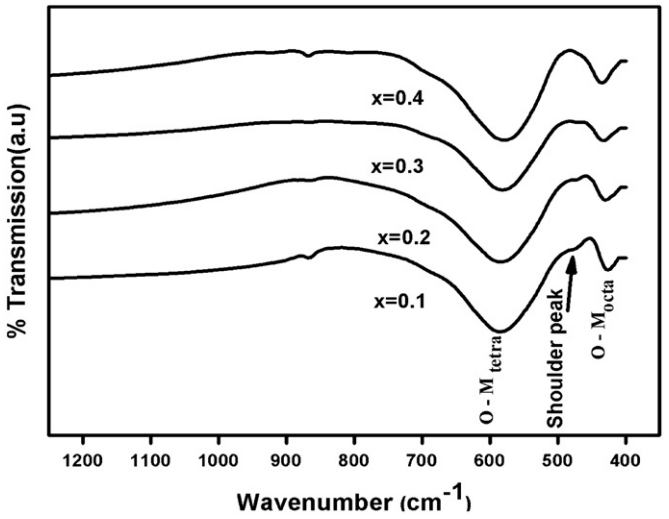

Fig. 3. Fourier Transform Infrared spectra of sintered $Ni_{0.5-x}Mg_xCu_{0.05}Zn_{0.45}Fe_2O_4$ ($x=0.1$, 0.2, 0.3, and 0.4) ferrite samples.

Table 1
Lattice constant, crystallite size, bulk density, grain size and IR frequency bands of $Ni_{0.5-x}Mg_xCu_{0.05}Zn_{0.45}Fe_2O_4$ ($x=0.1$, 0.2, 0.3, and 0.4) ferrite samples.

Composition x	Lattice Constant (Å)	Crystallite size (nm)	Bulk density (g/cm^3)	Grain size (nm)	ν_1 (cm^{-1})	ν_2 (cm^{-1})
0.1	8.3820	56	4.1764	72	585	426
0.2	8.4053	62	3.8048	137	584	430
0.3	8.3985	50	3.5121	153	581	433
0.4	8.4141	59	3.4854	219	579	435

decreasing trend with Mg composition. The reason being low atomic weight of Mg (24.305 amu) compared to Ni (58.6934 amu) and also density of Mg (1.74 g/cm^3) is lower than Ni (8.91 g/cm^3) [11].

Average crystallite size (D) for the samples is calculated from the peak broadening of the highest intensity (311) peak using Debye–Scherrer's formula

$$D = \frac{0.9\lambda}{\beta\cos\theta}$$

where λ is the wavelength of X-rays used (1.78897 Å), β is the full width at half maximum after applying correction due to instrumental broadening $\sqrt{\beta_{FWHM}^2-\beta_o^2}$. The instrumental broadening factor (β_o) is 0.07° obtained from the peak width of the coarse grained silica sample and θ is the Bragg's diffraction angle. The values of lattice constant, crystallite size, bulk density, grain size along with the IR frequency bands are presented in Table 1.

3.2. Fourier Transform Infrared spectral analysis (FTIR)

IR spectroscopy is an excellent tool to study the distribution of the cations in tetrahedral and octahedral sites in the ferrite system. It is also useful to determine the local symmetry in crystalline solids, ordering phenomenon in spinels and presence/absence of Fe^{2+} ions [22]. IR spectra of the samples showed two prominent bands ν_1 and ν_2 (Fig. 3). The higher frequency band ν_1 is assigned to oxygen–tetrahedron and Fe–O stretching vibrations. The lower frequency band ν_2 is assigned to oxygen–octahedron and O–Fe–O bending vibrations [23]. The frequency bands ν_1 and ν_2 are attributed mainly to Fe^{3+} (A/B)–O^{2-} vibrations because these ions have the highest valency (+3) in the spinel structure [22]. The frequency bands ν_1 and ν_2 for the present samples are in the wave number range of 585–579 cm^{-1} and 426–435 cm^{-1} respectively with Mg substitution. The change in the band positions of ν_1 and ν_2 is because of change in the bond length of Fe^{3+}–O^{2-} at tetrahedral (0.189 nm) and octahedral (0.199 nm) sites respectively [24]. The bands ν_1 and ν_2 are varying with Mg substitution since these are known to be affected by method of preparation, grain size and sintering temperature [25]. The observed bands (ν_1, and ν_2) are broad indicating inverse spinel structure, in which Fe^{3+} ions are distributed statistically at tetrahedral and octahedral sites based on the stoichiometric composition [26]. In addition to these strong bands there is a weak band observed around 470 cm^{-1} whose intensity decreased with Mg substitution. This is attributed to the presence of Jahn Teller Fe^{2+} ions in the ferrite samples. The presence of Fe^{2+} ions creates non-cubic crystal field potential which causes splitting of frequency bands [27].

Raghavender et al. [28] also noticed similar type of frequency band in between ν_1 and ν_2 absorption bands in IR spectra of $NiZnFe_2O_4$ system and they attributed it to the presence of small traces of α-Fe_2O_3 (haematite). They confirmed the presence of Fe_2O_3 by comparing the observed infrared spectra with pure Fe_2O_3 spectra. John Berchmans et al. [11] observed similar type of variations in ν_1 and ν_2 with Mg substitution in place of Ni and also noticed a subsidiary frequency band around 471 cm^{-1}, similar to the present results. Singh et al. [14] studied $Ni_{0.5-x}Mg_xZn_{0.5}Fe_2O_4$ system and infrared spectral analysis showed two strong peaks along with a low intensity peak around 470 cm^{-1} and they attributed it to vibration of Fe^{2+}–O^{2-} bond at octahedral sites. The band at 470 cm^{-1} has maximum intensity for the sample with $x=0.2$ and its intensity decreases gradually with Mg concentration ($x>0.2$) indicating reduced concentration of Fe^{2+} ions in the samples.

The frequency band ν_1 decreases with increasing Mg substitution. This is due to improved unit cell (a) dimensions resulting in increased bond length. Whereas the frequency band ν_2 increases with composition due to Mg (0.72 Å) of higher ionic radius substituted for Ni (0.69 Å) at octahedral sites which pushes Fe^{3+} towards O^{2-} ions resulting in reduced bond length thereby ν_2 increases.

3.3. Microstructural analysis

Fig. 4(a), (b), (c) and (d) displays morphology and microstructures of the $Ni_{0.5-x}Mg_xCu_{0.05}Zn_{0.45}Fe_2O_4$ ferrite samples with different Mg contents ($x=0.1$, 0.2, 0.3 and 0.4, respectively). The morphology of the sample with $x=0.1$ displayed homogeneous

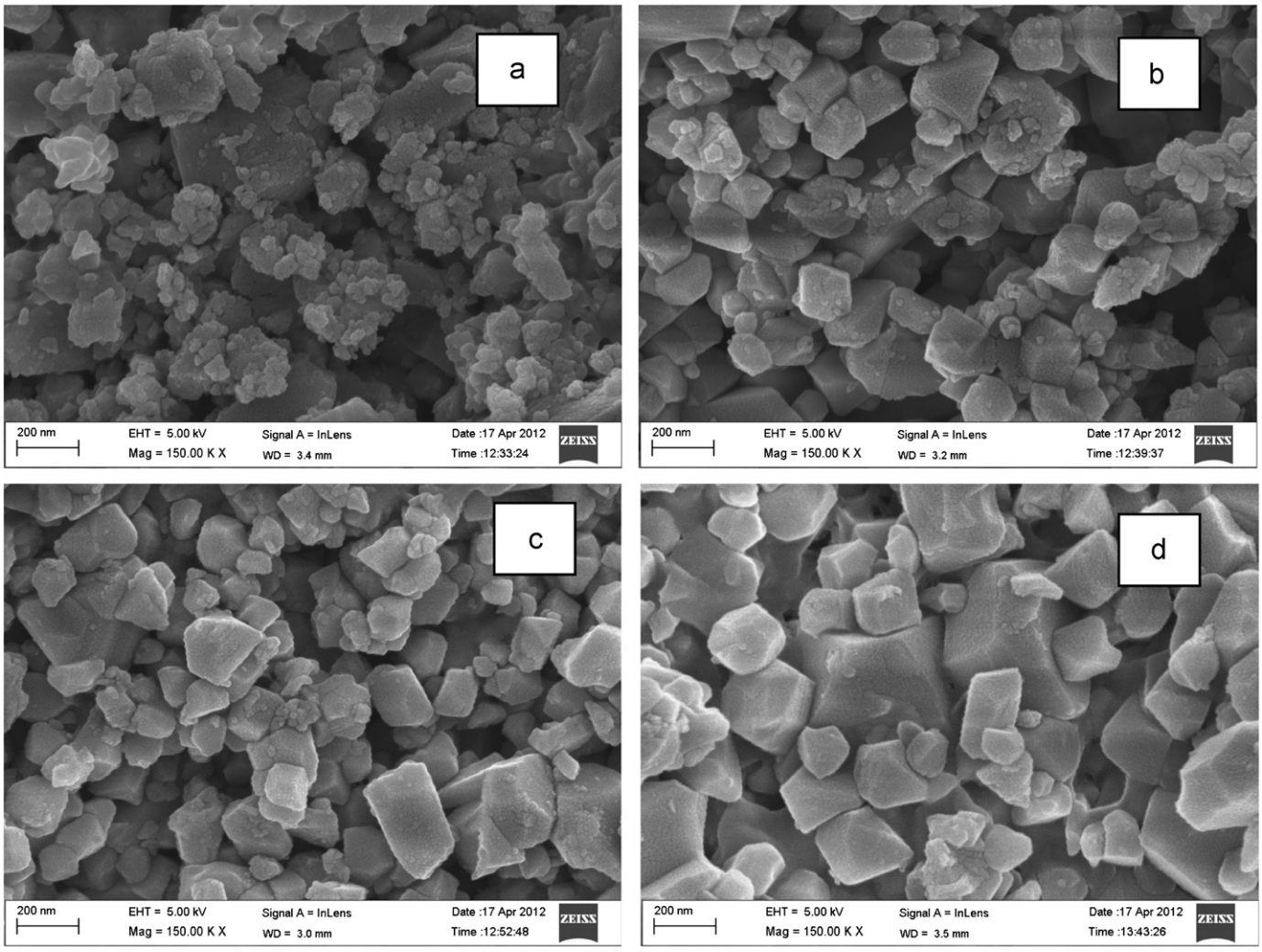

Fig. 4. Microstructures of the sintered $Ni_{0.5-x}Mg_xCu_{0.05}Zn_{0.45}Fe_2O_4$ ($x=0.1$, 0.2, 0.3, and 0.4) ferrite samples.

microstructure with small grain size (72 nm) having agglomerated as well as separated grains. Whereas the sample with $x=0.2$ showed polyhedral shaped grains with an average grain size of 137 nm. The microstructure of the sample ($x=0.2$) contains closed pores (not shown) due to the presence of divalent iron ions which causes discontinuous grain growth. The samples with $x=0.3$ and $x=0.4$ have an average grain size of 153 and 219 nm respectively. The microstructure for the sample with $x=0.3$ exhibits well defined grain boundaries having intergranular porosity with uniform grain size distribution. In case of the sample with $x=0.4$ there is an increased interaction among the grains. The observations showed an increased grain size with Mg composition. In general grain growth takes place mainly due to grain boundary diffusion since the activation energy for grain boundary diffusion is less than the lattice diffusion [29]. Swalin et al. [30] studied diffusion rates of different elements such as Mg, Si, and Mo in host Ni and found that Mg has low activation energy compared to other elements. Thus, Mg of low activation energy for diffusion is one of the reasons for improved grain size. The observations are in good agreement with the reported results [14].

3.4. Room temperature magnetic properties

Fig. 5 shows room temperature hysteresis loops for the sintered samples. The magnetic parameters such as saturation magnetisation (M_s), coercivity (H_c) and remanent magnetisation (M_r) obtained from the hysteresis loops are shown in Table 2. Hysteresis loops demonstrated soft ferrimagnetic nature of the samples and all the samples attaineded saturation within the limit of applied magnetic field. Saturation magnetisation M_s is known to

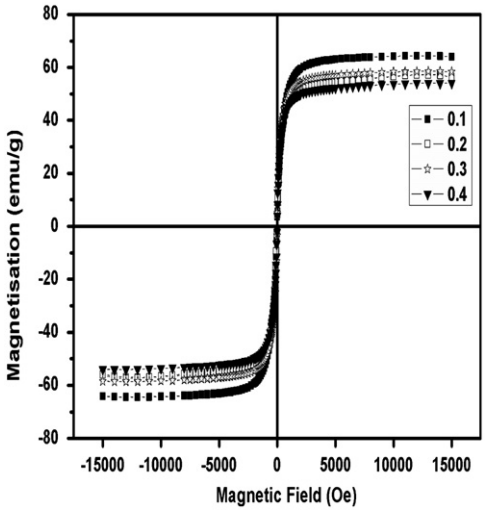

Fig. 5. Room temperature hysteresis loops for the sintered $Ni_{0.5-x}Mg_xCu_{0.05}Zn_{0.45}Fe_2O_4$ ($x=0.1$, 0.2, 0.3, and 0.4) ferrite samples.

be affected by both intrinsic (composition) and extrinsic factors (microstructure) [19]. In general the magnetic ordering in spinels is due to super exchange interactions among tetrahedral and octahedral metal ions through oxygen ions. In the present case as the Mg content increases A–O–B interactions became weak and hence saturation magnetisation decreases. According to Neel's molecular field model the AB super exchange interaction predominates the intra sublattice AA and BB interactions. Therefore net magnetic moment is given by the difference of magnetic moment of each sublattice i.e. $M=M_A-M_B$ [31]. Magnesium of 0 μ_B magnetic moment substituted for Nickel of 2.3 μ_B both having preference to occupy octahedral sites (B sites) reduces magnetic moment of the B sublattice, whereas magnetic moment of tetrahedral sublattice (A sites) remains unchanged. Thus, resultant magnetic moment and hence the magnetisation decreases monotonously with Mg substitution. Besides that increased lattice constant with Mg substitution causes increased distance among the cations which reduces AB exchange interactions is another reason for decreased magnetisation [32].

The intrinsic coercive force showed an increasing trend up to $x=0.2$ composition and decreases thereafter. The coercivity has a linear relationship with anisotropy constant and according to one ion model, the anisotropy of ferrites depends mainly on the amount of highly anisotropic Fe^{2+} ions in the sample [33]. In the present system stable divalent Mg ions substituted for Ni which is having an oxidation states of +2/+3, there may be a chance of Fe^{2+} ions at B sites in the system at lower concentrations of Mg (or higher concentration of Ni). As the concentration of Mg increases the concentration of Fe^{2+} ions at B sites reduces. The IR spectral data clearly showed reduced intensity of the band at 470 cm^{-1} with Mg substitution. Kester et al. [34] investigated oxidation reactions on mixed valence defect spinel ferrites and they found dependence of magnetic properties such as coercivity on oxidation states of the elements present in the samples. They observed improved coercivity when the sample contains cations with oxidation states of the type Cu^{1+} and Cu^{2+}, Fe^{2+} and Fe^{3+} or Mn^{3+} and Mn^{4+}. Thus in the present case increase of coercivity up to $x\leq0.2$ is due to presence of divalent iron ions in the samples. Anisotropy constant (K_1) is determined using the following relation [35].

$$K_1 = \frac{H_c M_{15\ \mathrm{kOe}}}{0.96}$$

From the values of anisotropy constant it is concluded that sample with composition $x=0.2$ has highest value compared to the remaining samples (Table 2). The variation of coercivity for the samples with $x>0.2$ is in accordance with the grains size. In case of multidomains coercivity varies inversely with the grain size [36].

$$H_c = e + \frac{f}{D}$$

where e and f are constants and D is the grain size. Thus the coercivity of the samples for $x>0.2$ are consistent with the reported results [37], where they reported dependence of coercivity on temperature and grain size.

Table 2
Saturation magnetisation, coercivity and anisotropy constant of $Ni_{0.5-x}Mg_xCu_{0.05}Zn_{0.45}Fe_2O_4$ ($x=0.1$, 0.2, 0.3, and 0.4) ferrite samples.

Composition x	Saturation magnetisation M_s (emu/g)	Coercivity H_c (Oe)	Anisotropy constant K_1 (erg/cm^3)
0.1	64.4	17	1140
0.2	57.4	23.5	1405
0.3	58.6	18.7	1141
0.4	54.1	8.6	484

3.5. Frequency dispersion of permeability

Frequency dispersion of permeability for the $Ni_{0.5-x}Mg_xCu_{0.05}Zn_{0.45}Fe_2O_4$ ferrite samples are shown in Fig. 6. The basic magnetisation contribution to the permeability is superposition of domain wall bulging, domain wall (DW) displacement and spin rotation magnetisation mechanisms. At low frequency range domain wall bulging and displacement contributions to the permeability are dominant. Domain wall bulging is of relaxation type and it depends on extent of pinning. Domain wall displacement is of resonance

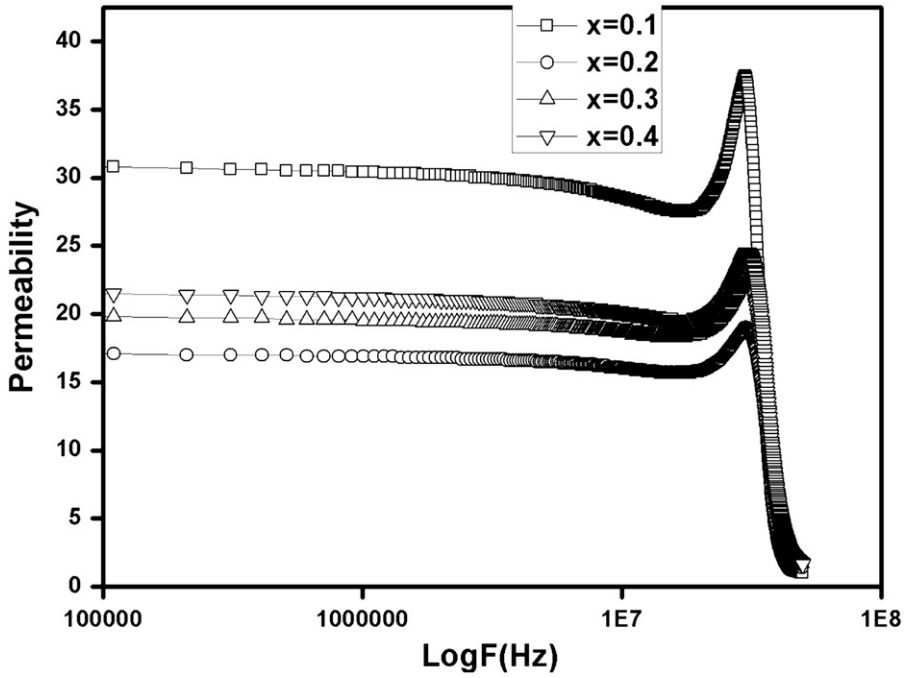

Fig. 6. Frequency dispersion of permeability for the sintered $Ni_{0.5-x}Mg_xCu_{0.05}Zn_{0.45}Fe_2O_4$ ($x=0.1$, 0.2, 0.3, and 0.4) ferrite samples.

type and its frequency increases as the width of the domain wall reduces [10]. Spin rotation occurs at higher frequency (GHz) since it is observed in single domain particles where the entire spins in the particle has to rotate in the applied field direction. In the present case the grain size is in μm range implies particles are in multi-domain state and hence the frequency dispersion of permeability spectra exhibits mixed behaviour of the type relaxation–resonance similar to the literature report [38]. Magnitude of permeability depends on saturation magnetisation, anisotropy constant, grain size and density of the material. The permeability is high for the sample at $x=0.1$ and decreases for $x=0.2$ and again increases. The high value of permeability for the sample $x=0.1$ is due to the fact that at this composition both magnetisation and density are high compared to all other samples. Compositional variation of permeability is shown in Fig. 7. Low value of permeability for the sample $x=0.2$ may be due to the presence of highly anisotropic divalent iron (Fe^{2+}) ions in the sample as well as due to porosity. Deka and Joy [39] discussed that chemical homogeneity, in particular presence of Fe^{2+} ions in fine sized grains is one of the factors affecting the permeability of the ferrites. The presence of these ions increases the magnetocrystalline anisotropy constant of the ferrites thereby permeability decreases. Magnetocrystalline anisotropy constant and magnetic permeability of Mn–Zn–Fe single crystals was studied by Ohta [40] and showed that permeability of the system reduces when it contains excess of iron ions (Fe^{2+}) at octahedral sites. They attributed it to the positive anisotropy constant of Fe^{2+} ions. After $x=0.2$ composition, the permeability is again raised and is due to increased grain size with Mg composition. As the grain size increases with Mg composition the grains are in multidomain state thereby easy domain wall motion was possible resulting in increased permeability. A similar type of study on Mg substituted NiCuZn ferrites prepared through chemical route method showed improved permeability up to $x=0.18$ and thereafter decreased [17]. The frequency dispersion of permeability spectrum shows a peak at one particular frequency indicating operating/cut off frequency of the material. The increase of permeability and decrease in cut off frequency with Mg composition is in good agreement with the Snoek's law. The observed cut off frequency for the present samples is higher than the reported NiMgCuZn ferrite system [17]. The samples exhibit high frequency stability of permeability up to 30 MHz frequency.

3.6. Dielectric properties

Room temperature dielectric measurements as a function of frequency are shown in Fig. 8. The dielectric constant was calculated using the formula

$$\in' = \frac{Ct}{\in_o A}$$

where C is the capacitance of the disc shaped pellet in pF, t is the thickness of the pellet, $\in_o$ is the permittivity of free space (8.85×10^{-12} F/m) and A is the cross-sectional area of the flat surface of the sample.

Dielectric properties mostly depend on preparation conditions like sintering temperature, time, type and quantity of additives [12]. The dielectric constant of all the studied samples is high at lower frequencies and decreases with frequency and becomes constant at higher frequency showing normal dielectric constant behaviour without any peak. This behaviour is attributed to space charge polarisation due to inhomogeneous microstructure. The large values of $\in'$ at lower frequency are attributed to Fe^{2+}, Cu^{+1} ions, interfacial dislocation pile ups, oxygen vacancies and grain

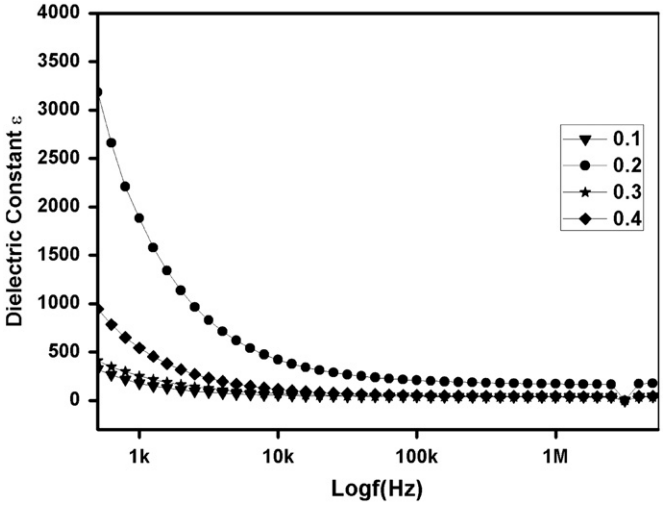

Fig. 8. Dielectric constant versus frequency for the sintered $Ni_{0.5-x}Mg_xCu_{0.05}Zn_{0.45}Fe_2O_4$ ($x=0.1$, 0.2, 0.3, and 0.4) ferrite samples.

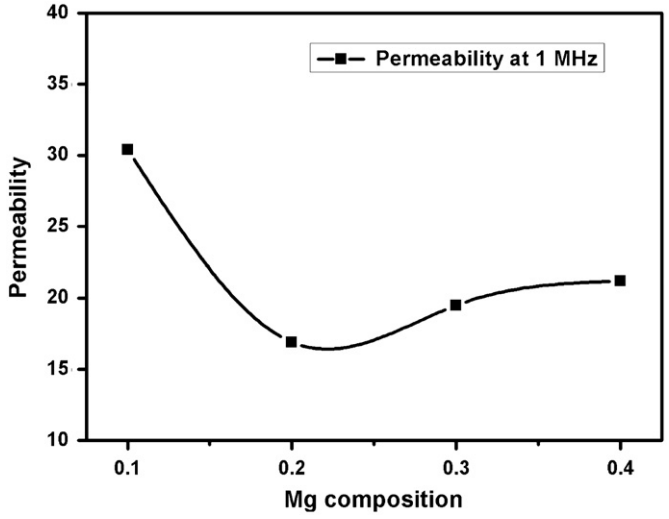

Fig. 7. Compositional variation of permeability for the sintered $Ni_{0.5-x}Mg_xCu_{0.05}Zn_{0.45}Fe_2O_4$ ($x=0.1$, 0.2, 0.3, and 0.4) ferrite samples.

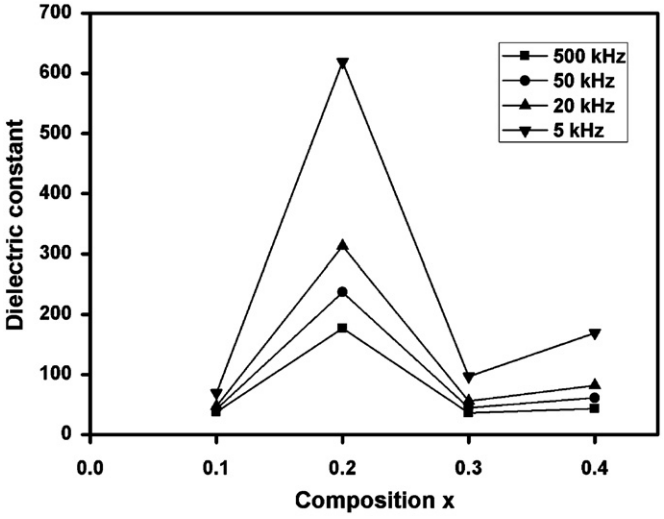

Fig. 9. Compositional variation of dielectric constant of sintered $Ni_{0.5-x}Mg_xCu_{0.05}Zn_{0.45}Fe_2O_4$ ($x=0.1$, 0.2, 0.3, and 0.4) ferrite samples at different frequencies.

boundary defects [41]. The sample with composition $x=0.2$ has the highest dielectric constant compared to all other samples due to the presence of higher concentration of Fe^{2+} ions. The presence of these ions in the sample and their displacement with the applied electric field is responsible for the polarisation in ferrites resulting in increased dielectric constant [12]. A shoulder peak ($470\ cm^{-1}$) in FTIR spectra as discussed earlier confirmed the presence of divalent iron ions. Dielectric constant with composition at different frequencies is shown in the Fig. 9.

Fig. 10 shows room temperature ac conductivity curves with frequency for the samples with $x=0.1$, 0.2, 0.3 and 0.4. All the samples showed increase in conductivity with frequency since as the applied frequency increases, probability for jumping of electron through Fe^{3+}/Fe^{2+} ions increases. The ac conductivity of the samples were calculated from dielectric parameters using the formula

$$\sigma_{ac} = \in_o \in' \tan\delta\ \omega$$

where $\tan\delta$ is the dielectric loss factor and ω is the applied frequency. Conduction mechanism in ferrites is mainly due to the hopping of electrons between iron ions which are existed in different oxidation states. The observations showed both ac conductivity and dielectric constant have similar trend with increasing Mg substitution confirming linear relationship between them. The highest value of conductivity for the sample with $x=0.2$ provides evidence for the existence of divalent iron ions at that particular Mg content.

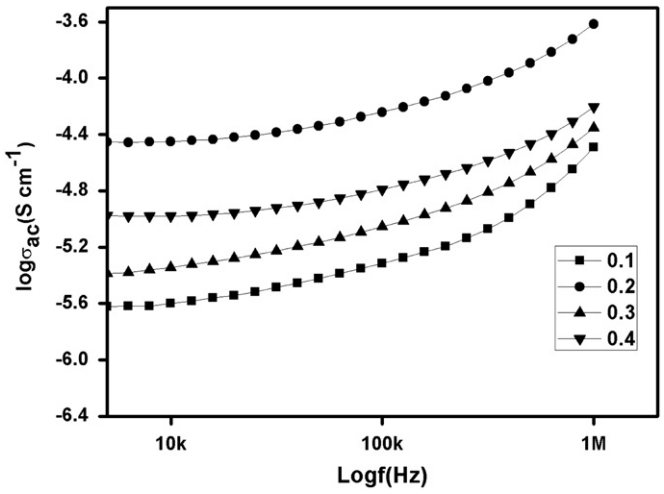

Fig. 10. AC conductivity versus frequency for the sintered $Ni_{0.5-x}Mg_xCu_{0.05}Zn_{0.45}Fe_2O_4$ ($x=0.1$, 0.2, 0.3, and 0.4) ferrite samples.

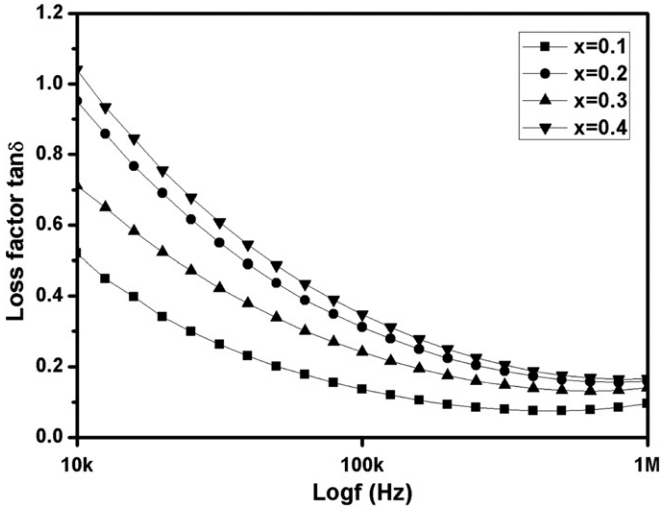

Fig. 11. Dielectric loss factor $\tan\delta$ versus frequency for the sintered $Ni_{0.5-x}Mg_xCu_{0.05}Zn_{0.45}Fe_2O_4$ ($x=0.1$, 0.2, 0.3, and 0.4) ferrite samples.

Fig. 11 shows variation of dielectric loss factor $\tan\delta$ for the samples as a function of frequency at room temperature. It is observed that $\tan\delta$ showed similar trend as that of dielectric constant with frequency. The loss factor has high values at low frequencies for each composition, since the applied frequency is smaller than the hopping frequency, thus electrons follow the field and hence the loss is maximum whereas at higher frequencies the electrons lag behind the field and the loss was minimum [42].

4. Conclusions

Mg substituted NiCuZn ferrite with $x=0.1$, 0.2, 0.3 and 0.4 samples were prepared successfully through sol–gel method using polyvinyl alcohol as a chelating agent. All the samples showed single phase cubic spinel structure with increased grain size as a function of Mg substitution. The IR frequency band signals the presence of divalent iron ions in the samples and the band intensity reduces with Mg composition. Saturation magnetisation showed decreasing trend with Mg substitution for Ni. The intrinsic coercivity has maximum at $x=0.2$ due to presence of Fe^{2+} ions and decreases after that. Dielectric properties of the samples showed normal ferrimagnetic behaviour with maximum value of dielectric constant for the sample at $x=0.2$. The initial permeability is maximum for the sample $x=0.1$. Mg substituted for Ni manifested improved microstructure and permeability and reduced dielectric losses at higher frequencies.

Acknowledgements

Authors would like to express their gratitude towards Prof. C. Bansal, Dean, School of Physics, University of Hyderabad for providing the XRD and FESEM facility. Also the authors are very much thankful to Mr. Y.B. Ravi Shankar and Mr. Laxman for their help in taking XRD and FESEM data.

References

[1] M. Kaiser, Current Applied Physics 10 (2010) 975.
[2] M. Penchal Reddy, W. Madhuri, N. Ramamanohar Reddy, K.V. Siva Kumar, V.R.K. Murthy, R. Ramakrishna Reddy, Materials Science and Engineering C 30 (2010) 1094.
[3] M.A. Gabal, Y.M. Al Angari, S.S. Al-Juaid, Journal of Alloys and Compounds 492 (2010) 411.
[4] Qi Xiwei, Ji Zhou, Yue Zhenxing, Gui Zhilun, Li Longtu, Journal of Magnetism and Magnetic Materials 251 (2002) 316.
[5] M. Saidani, M.A.M. Gijs, Applied Physics Letters 84 (2004) 4496.
[6] M. Penchal Reddy, W. Madhuri, G. Balakrishnaiah, N. Ramamanohar Reddy, K.V. Siva Kumar, V.R.K. Murthy, R. Ramakrishna Reddy, Current Applied Physics 11 (2011) 191.
[7] Sagar E. Shirsath, R.H. Kadam, S.M. Patange, M.L. Mane, Ali Ghasemi, Akimitsu Morisako, Applied Physics Letters 100 (2012) 042407.
[8] Hua Su, Huaiwu Zhang, Xiaoli Tang, Baoyuan Liu, Zhiyong Zhong, Journal of Alloys and Compounds 475 (2009) 683.
[9] A. Daigle, J. Modest, A.L. Geiler, S. Gillette, Y. Chen, M. Geiler, B. Hu, S. Kim, K. Stopher, C. Vittoria, V.G. Harris, NANOTECHNOLOGY 22 (2011) 305708.
[10] Ch. Sujatha, K. Venugopal Reddy, K. Sowri Babu, A. RamaChandra Reddy, K.H. Rao, Ceramics International 38 (2012) 5813.
[11] L. John Berchmans, R. Kalai Selvana, P.N. Selva Kumar, C.O. Augustin, Journal of Magnetism and Magnetic Materials 279 (2004) 103.
[12] Muddassar Naeem, Nazar Abbas Shah, Iftikhar Hussain Gul, Asghari Maqsood, Journal of Alloys and Compounds 487 (2009) 739.
[13] V.K. Mittal, P. Chandramohan, Santanu era, M.P. Srinivasan, S. Velmurugan, S.V. Narasimhan, Solid State Communications 137 (2006) 6.
[14] Navneeth Singh, Ashish Agarwal, Sujata Sanghi, Paramajeet Singh, Physica B 406 (2011) 687.
[15] N. Rezlescu, E. Rezlescu, P.D. Popa, M.L. Craus, L. Rezlescu, Journal of Magnetism and Magnetic Materials 182 (1998) 199.
[16] Narla Varalaxmi, N. Ramamanohar Reddy, Mudinepalli Venkata Ramana, Eyunni Rajagopal, V. Ramakrishna Murthy, Kota Venkata Sivakumar, Journal of Materials Science: Materials in Electronics 19 (2008) 399.

[17] P.K. Roy, J. Bera, Journal of Magnetism and Magnetic Materials 298 (2006) 38.
[18] Hua Su, Huaiwu Zhang, Xiaoli Tang, Yulan Jing, Baoyuan Liu, IEEE Transactions on Magnetics 45 (5) (2009) 2050.
[19] M.A. Gabal, Journal of Magnetism and Magnetic Materials 321 (2009) 3144.
[20] M. Abdullah Dara, Vivek Verma, S.P. Gairola, W.A. Siddiqui, Rakesh Kumar Singh, R.K. Kotnal, Applied Surface Science 258 (2012) 5342.
[21] Ch. Sujatha, K. Venugopal Reddy, K. Sowri Babu, A. RamaChandra Reddy, K.H. Rao, Physica B 407 (2012) 1232.
[22] Rajesh Iyer, Rucha Desai, R.V. Upadhyay, Indian Journal of Pure and Applied Physics 47 (2009) 180.
[23] Osama Mohamed HEMEDA, Monsen Mohmed BARAKAT, Dalal Mohamed HEMEDA, Turkish Journal of Physics 27 (2003) 537.
[24] K.B. Modi, U.N. Trivedi, P.U. Sharma, V.K. Lakhani, M.C. Chhantbar, H.H. Joshi, Indian Journal of Pure and Applied Physics 44 (2006) 165.
[25] B.K. Labde, Madan C. Sable, N.R. Shamkuwar, Materials Letters 57 (2003) 1651.
[26] S.A. Patil, V.C. Mahajan, A.K. Ghatage, S.D. Lotke, Materials Chemistry and Physics 57 (1998) 86.
[27] T.K. Pathak, N.H. Vasoya, V.K. Lakhani, K.B. Modi, Ceramics International 36 (2010) 275.
[28] A.T. Raghavender, N. Biliškov, Ž. Skoko, Materials Letters 65 (2011) 677.
[29] Dean-Mo Liu, Journal of Materials Science 29 (1994) 1507.
[30] R.A. Swalin, Allan Martin, R. Olson, JOM (1957) 936.
[31] Y.P. Fu, C.H. Lin, Journal of Applied Physics 105 (2009) 07A505.
[32] Brian T. Naughton, David R. Clarke, Journal of the American Ceramic Society 90 (2007) 3541.
[33] A.A. Sattar, H.M. EI-Sayed, K.M. EI-Shokrofy, M.M. EI-Tabey, JMEPEG 14 (2005) 99.
[34] E. Kester, P. Perriat, B. Gillot, Ph. Taihades, A. Rousset, Solid State Ionics 101 (1997) 457.
[35] P.A. Shaikh, R.C. Kambale, A.V. Rao, Y.D. Kolekar, Journal of Alloys and Compounds 492 (2010) 590–596.
[36] Lawrence Kumar, Manoranjan Kar, Ceramics International 38 (2012) 4771.
[37] Azadeh Ashrafizadeha, Ali Ghasemi, Andrea Paesano Jr., Carla Fabiana Cerqueira Machado, Xiaoxi Liu, Akimitsu Morisako, Journal of Alloys and Compounds 506 (2010) 279.
[38] G. Herrera, Journal of Applied Physics 108 (2010) 103901.
[39] Sasanka Deka, P.A. Joy, Journal of the American Ceramic Society 90 (5) (2007) 1494.
[40] Keizo OHTA, Journal of the Physical Society of Japan 18 (1963) 685.
[41] U.N. Trivedi, M.C. Chhantbar, K.B. Modi, H.H. Joshi, Indian Journal of Pure and Applied Physics 43 (2005) 688.
[42] E. Melagiriyapp, H.S. Jauanna, B.K. Chougule, Materials Chemistry and Physics 112 (2008) 68.